

## NEW FATIGUE DATA FOR WIND TURBINE BLADE MATERIALS

John F. Mandell, Daniel D. Samborsky, Lei Wang  
Montana State University  
Bozeman, Montana 59717  
and

Neil K. Wahl  
Montana Tech of the University of Montana  
Butte, Montana 59701

### **ABSTRACT**

This paper reports on recent fatigue data of interest to the wind turbine industry in several areas: (a) very high cycle S-N data; (b) refined Goodman Diagram; (c) effects of fiber waviness; and (d) large tow carbon fibers. Tensile fatigue results from a specialized high frequency small strand testing facility have been carried out to  $10^{10}$  cycles in some cases, beyond the expected cycle range for turbines. While the data cannot be used directly in design due to the specialized test specimen, the data trends help to clarify the proper models for extrapolating from standard coupons to higher cycles. The results for various fiber and matrix systems also provide insight into basic failure mechanisms. For spectrum loading predictions, a more detailed Goodman Diagram has been developed with additional R-values (R is the ratio of minimum to maximum stress in a cycle). The data of greatest interest were obtained for tensile fatigue with low cyclic amplitudes, close to  $R=1.0$ , to clarify the shape of the diagram as the cyclic amplitude approaches zero. These data may significantly shorten lifetime predictions compared with traditional Goodman Diagram constructions based on more limited data.

The effects of material/process induced flaws on properties continues to be a major concern, particularly with large tow carbon fabrics. The results of a study of fiber waviness effects on compressive strength show significant strength reductions for severe waviness which can be introduced in resin infusion processes. The final section presents new fatigue results for large tow carbon/fiberglass hybrid composites. Epoxy resin laminates show marginally higher compressive strength and fatigue resistance with carbon fibers. Improved compressive static and fatigue performance is found with stitched fabrics as compared with woven fabrics.

### **INTRODUCTION**

This paper presents static and fatigue test results in

---

This research was supported by Sandia National Laboratories under subcontract BC7159. \*Copyright © 2003 by the American Institute of Aeronautics and Astronautics Inc., and the American Society of Mechanical Engineers. All rights reserved.

four distinct areas: (a) very high cyclic tension fatigue; (b) refinements to the Goodman Diagram in the low amplitude tension regime; (c) effects of fiber waviness on compression properties; and (d) large tow carbon laminates. Each section is self-contained and independent of the other sections.

### **VERY HIGH CYCLE TESTING AND RESULTS**

#### **Introduction**

Composite wind turbine blade materials may experience between  $10^8$  to  $10^9$  significant fatigue cycles in their 20 to 30 year lifetime. The design of wind turbines has required use of extrapolations from experimental data due to the lack of data beyond  $10^7$  or  $10^8$  cycles, with little guidance as to appropriate extrapolation models. A spectrum fatigue investigation reported earlier [1, 2] showed two interesting features relating to high cycles. First, significant sensitivity to the fatigue model assumed in fitting the constant amplitude data [2-4], and second, many of the stresses in the spectrum for overall lifetimes of  $10^6$  to  $10^7$  cycles were in the low stress range where no fatigue data exist. Thus, the damage contribution to be assigned to the low stress cycles requires extrapolation of the S-N data.

To be practical, testing to high cycles requires high frequencies, and high frequencies can only be used for very small specimens to avoid hysteretic heating and thermal failure of the polymer based composite [5]. This study involved very small diameter impregnated strands with only enough fibers to be representative of the behavior of larger specimens (when tested at moderate cycles). Limitations have also existed on testing equipment. Standard servo-hydraulic machines are limited in their frequency, and the actuator rod assembly also has wearing problems; piezoelectric actuators have displacement and thermal limitations, and standard vibration table equipment can be costly. In order to determine the high cycle behavior of impregnated glass strands, it was necessary to build a unique low cost testing apparatus with several test stations.

**Experimental Methods**

The fiber testing apparatus uses various low frequency audio speakers (woofers) as actuators which can handle frequencies as high as 300 Hz. The speakers were 25 to 30 cm in diameter with audio handling capabilities greater than 100 watts. These speakers can deliver a maximum force of approximately 25 N with a displacement of approximately  $\pm 5$  mm. The force capacity allows a strand containing 45 E-glass fibers to be tested. Earlier studies have shown fatigue S-N (maximum stress versus cycles to failure) response similar to laminates when 30 fibers are used [4, 6, 7]. A total of five test stations were constructed. The test apparatus and gripping are shown in Figure 1; References 4, 8 and 9 contain further testing details.

The test strands consisted of small strands containing 45 E-glass fibers with an average fiber diameter of 10.6  $\mu\text{m}$ , carefully removed from an Owens Corning Fabrics, OC-990-BC-2385-4093 roving. These strands were then drawn through a bath of resin and suspended vertically to cure. The final coupon diameter was between 0.09 and 0.1 mm, with an average fiber volume fraction of 0.55. The resin for most tests was an unsaturated orthophthalic polyester resin, CoRezyn 63-AX-051, obtained from Interplastic Corporation. Additional tests were run on the same strands with a Derakane 8084 toughened vinyl ester resin. The cured strands were cut to length and bonded to 75  $\text{g}/\text{m}^2$  paper tabs using silicone sealant and a structural adhesive, Hysol EA9309.2NA, as shown in Figure 2. The gage length of the strand is 25 mm. The silicone rubber reduces the stress concentration as the strand enters the tab. The final specimens were post cured at 60°C for 2 hours.

Static tests were performed by attaching a 12.6 volt battery across the speaker terminals (4 ohms), which drove the speaker at a reproducible displacement rate of 140 to 150 mm per second, similar to the displacement rate in fatigue. This produced strand failures in approximately five to ten milliseconds. Fatigue tests were run with a sinusoidal waveform at the highest frequency possible, which was generally limited to 200 Hz due to the acoustical noise. No surface temperature increase was noticeable, as initially monitored by temperature sensitive paints. Coupon failure was defined as the inability of the coupon to hold the prescribed maximum load, which usually coincided with complete fracture of the strand. Coupons which were stopped prior to failure are termed “run outs”.

The control mode of the apparatus was modified position control, where the cyclic load was manually adjusted throughout the test to best maintain the loads. Most tests only required daily adjustments. Loads were

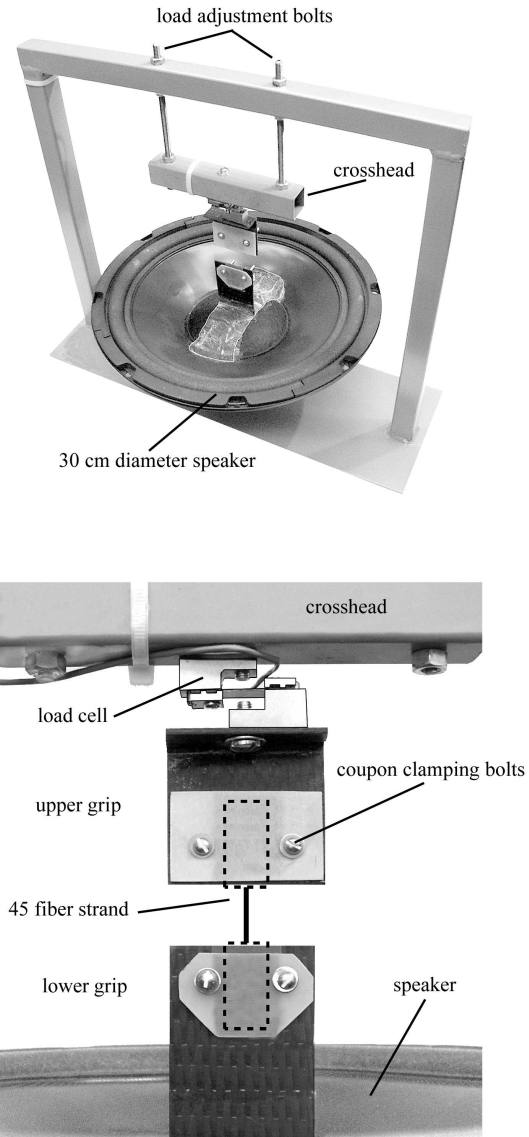


Figure 1. Small Strand Test Apparatus.

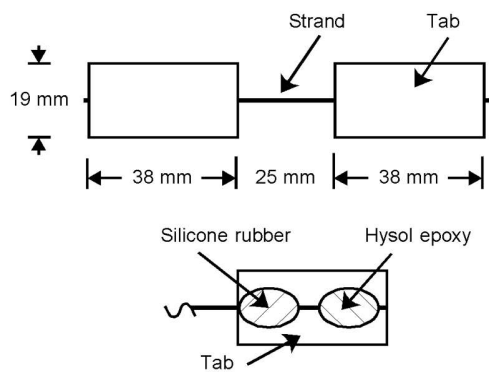


Figure 2. Small Strand Test Geometry.

monitored throughout selected tests, with typical maximum daily error in the maximum or minimum load under two percent. In position control, the applied load will drop if the coupon stiffness changes or the coupon slips in the gripping fixture. The frequency of the sinusoidal waveform was varied approximately inversely with the maximum stress level, giving an average displacement rate over a half-cycle of 110 mm/s; the lower frequencies at higher loads limited any hysteric heating.

After testing, a sample of the strand in the tab was removed for microscope examination for number of fibers in the strand and their diameters for calculation of the maximum stress; this determination of the cross-sectional area of the fibers was carried out for samples from every strand. Eight of the test coupons were found to deviate from the target 45 fibers in the gage section (ranging between 42 and 51 fibers); the applied load was adjusted linearly to normalize it to a fiber cross sectional area of 45 fibers. An average cross-sectional fiber area was used in the normalization, since all the coupons were manufactured from the same individual fibers, just at different locations along the length of a 12 meter long roving.

## **Results and Discussion**

Most of the coupons failed in the gage section, with significant fiber failures (brooming) and transverse matrix cracks. The polyester resin used to impregnate these fibers had an ultimate strain to failure of approximately 2.0 percent [10], and the test coupons showed numerous transverse matrix cracks along the length of the strand. The coupons which were run-outs showed no noticeable matrix cracking or broken fibers in the gage section.

The S-N data are presented in Figures 3 to 5, in terms of fiber stress, normalized stress and strain. The high strength and strain to failure of the small strands is also extended to the fatigue resistance, with very high strain levels at high cycles, and a less-steep S-N trend than for larger coupons at similar fiber content.

Figures 6 and 7 compare the normalized S-N data plotted linear-log and log-log, respectively, with exponential (Equation 1) and power law (Equation 2) curve fits (including static data, not including runouts).

$$\frac{S}{S_0} = A - b \text{Log } N \quad (1)$$

$$\frac{S}{S_0} = BN^{-\frac{1}{n}} \quad (2)$$

where

S = maximum cyclic stress

S<sub>0</sub> = single cycle (static) strength

N = cycles to failure

A, b, B, n = constants

The curve-fit equations are shown on the graphs. The power law trend fits the data well, including run-outs. The exponential trend fits only if a fatigue limit or slope decrease around 10<sup>8</sup> cycles is included. A combination of exponential fit at lower cycles and power law fit at higher cycles is shown in Figure 8.

Larger strands, taken from D155 fabric, containing 2000 fibers (Owens-Corning OC 107B-AC-450) were also impregnated with the ortho-polyester resin and tested. These were tested in an Instron 8511 servo-hydraulic machine at a maximum frequency of 80 Hz. Figure 9 shows the larger strand data, extending to between 10<sup>8</sup> and 10<sup>9</sup> cycles, fit with the exponential and power law models. The data are similar to the smaller strand data in Figure 6. Figure 10 contains a combined plot of the two data sets. The larger strand data show a slight reduction in slope in the 10<sup>8</sup> to 10<sup>9</sup> cycle range on a semi-log plot. The large strand data tend to validate the trends for the smaller strands, which can be run to higher cycles due to the higher frequencies (the small strand tests required 579 days to reach 10<sup>10</sup> cycles).

Comparison of these data with earlier results for standard coupons in the DOE/MSU Database using the same strands in unidirectional D155 fabric composites is shown in Figure 11. The larger coupons show a lower strain. The laminate results also depend on the fiber content as discussed in Reference 4, with the lower fiber content showing a normalized exponential S-N slope, b, of about 0.10. This is the lowest slope measured for glass fiber materials in standard coupons [4, 5, 7]. The strand data show somewhat less steep S-N trends in addition to the higher static strains.

Use of the strand data in blade design is problematical, due to the size effects shown in Figure 11. At 10<sup>6</sup> cycles, the small strand strains are about 2.0 percent, while the best of the standard coupon materials give a strain in the range of 1.2 percent, and the laminates with higher fiber contents are in the range of 0.6 percent [4]. Thus, it would be wrong to use the small strand data to establish allowable strains for design. However, the small strand data may be useful in establishing the best choice for a curve fit model, exponential versus power law. The power law fit appears to be the best choice at this time, as evidenced in Figure 7.

The small strand tests may also be useful in exploring factors such as matrix selection for high cycle fatigue resistance. Figure 12 presents data for the toughened vinyl ester resin Derakane 8084, compared with the

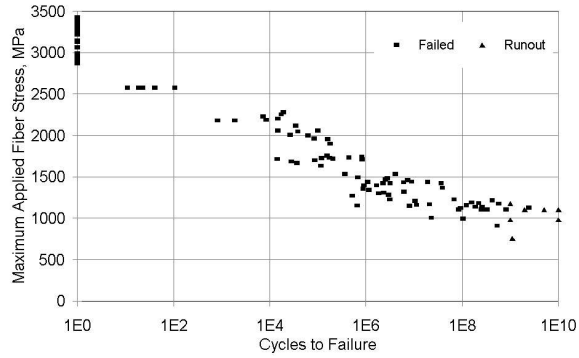


Figure 3. Maximum Applied Fiber Stress versus Log Cycles for Small Strands, R = 0.1 (using measured cross-sectional area of glass fibers only, excluding resin).

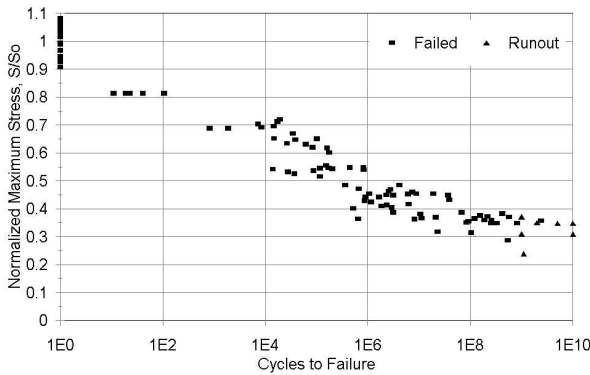


Figure 4. Normalized Maximum Stress versus Log Cycles Diagram for Small Strands, R = 0.1.

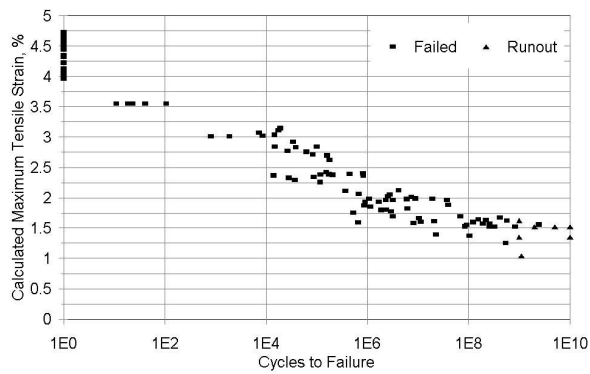


Figure 5. Calculated Maximum Tensile Strain versus Log Cycles for Small Strands, R = 0.1 (strain calculated by dividing maximum fiber stress by the fiber elastic modulus, 72.4 GPa).

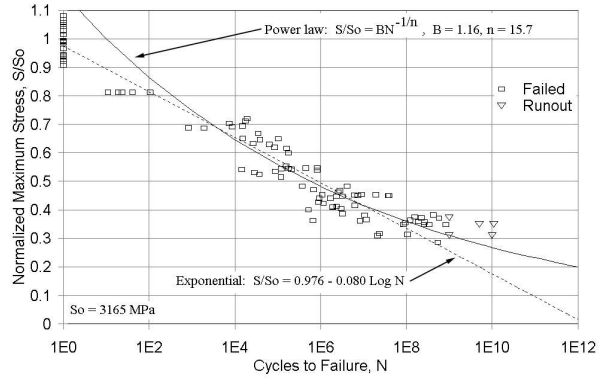


Figure 6. Normalized Tensile Stress versus Log Cycles for Small Strands with Trend Lines.

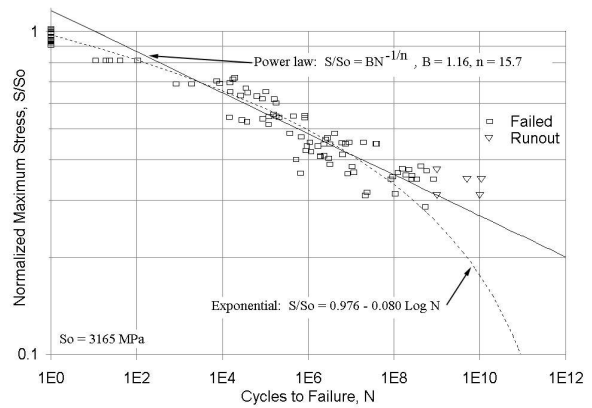


Figure 7. Log Normalized Tensile Stress versus Log Cycles for Small Strands with Trend Lines.

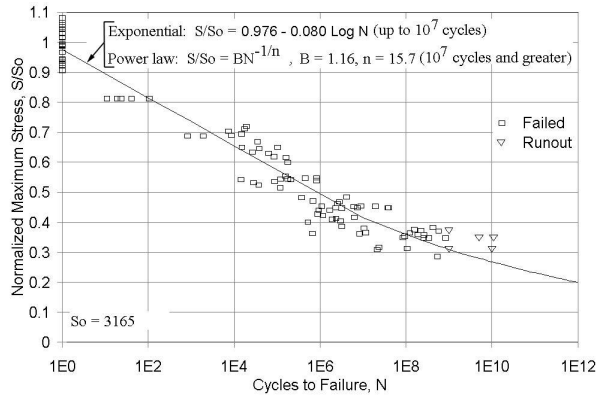


Figure 8. Normalized Tensile Stress versus Log Cycles for Small Strands with Combined Trend Line.

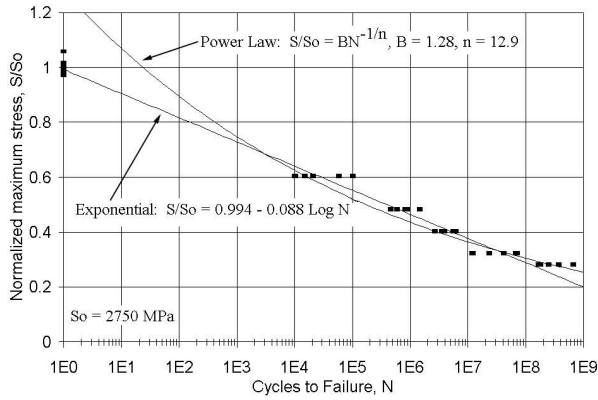


Figure 9. Normalized Fatigue Diagram for D155 Strands with 2000 Fibers.

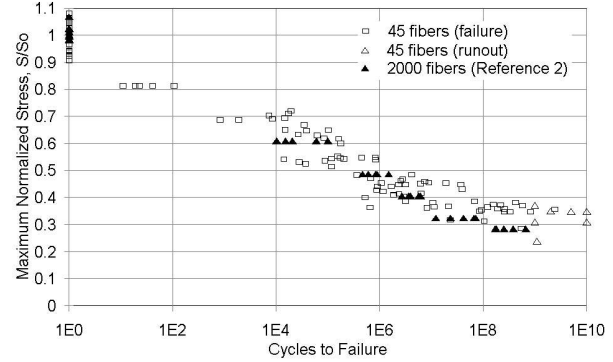


Figure 10. Normalized Fatigue Diagram for Small Strands with 45 Fibers Compared with Larger 2000 Fiber Strands.

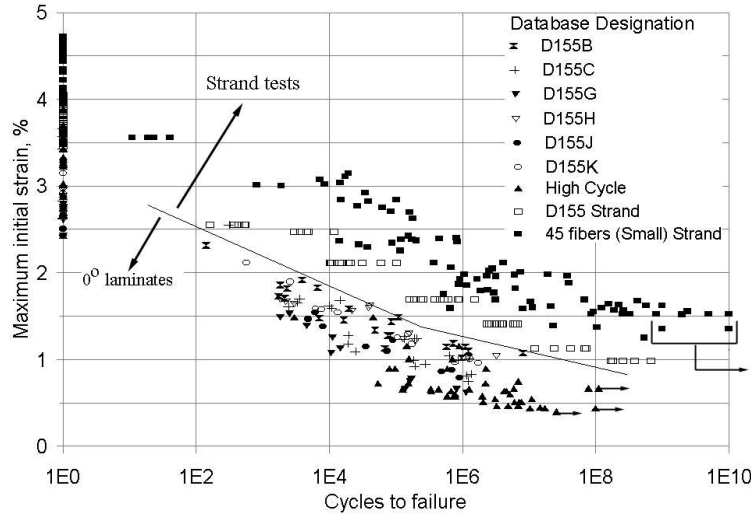


Figure 11. Maximum Initial Tensile Strain for Laminates and Small Strands, R = 0.1.

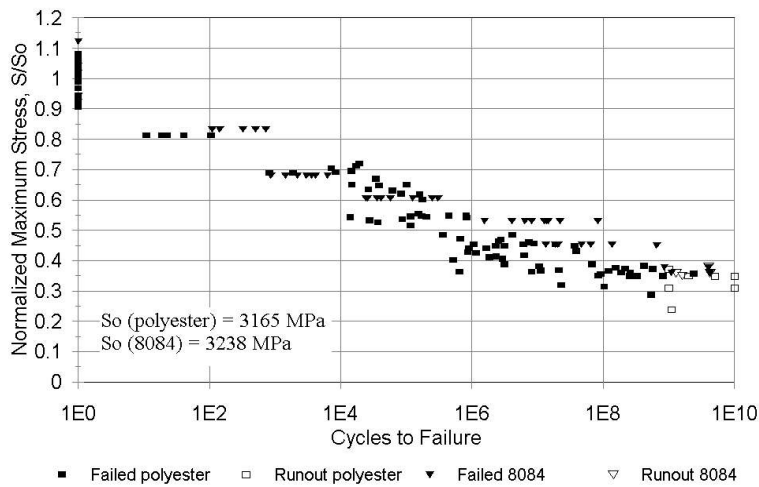


Figure 12. Normalized Maximum Stress versus Log Cycles for Polyester and Vinyl Ester Impregnated Small Strands, R = 0.1.

baseline orthophthalic polyester. The vinyl ester has higher toughness and strain to failure, but approximately the same elastic modulus as the polyester [10]. The data in Figure 12 indicate only a slight improvement with the 8084 resin at cycles above  $10^6$ . As reported earlier for many systems [4, 5], the matrix has little effect on tensile fatigue resistance out to  $10^6$  cycles using conventional coupons.

## **GOODMAN DIAGRAM**

### **Introduction**

Previous reports [2, 3, 11-13] have shown a very limited ability to predict spectrum fatigue lifetime from constant amplitude fatigue data. Predictions based on Miner's Rule are sometimes non-conservative by a factor of ten in lifetime, and other cumulative damage theories provide very limited improvement for wind turbine spectra. Lifetime predictions are based on interpolations within a Goodman Diagram plot of amplitude versus mean stress, where constant amplitude test data at a particular R-value (min. stress/max. stress) plot as a straight line. Goodman Diagrams may be constructed from many data sets at various R-values, or from as few as one dataset at  $R=-1$ , combined with static ultimate strength data for the zero-amplitude intercepts [13, 14].

Two factors can complicate Goodman Diagrams for composite materials. First, the failure modes can change significantly with R-value, particularly in the stress domain where the dominant mode shifts between tension to compression, near  $R=-1.0$ . Second, the static strengths in tension and compression are strongly dependent on the timescale of loading, so the intercept at zero-amplitude ( $R=1.0$ ) is uncertain. In a recent paper, van Delft, et.al. [13] showed that the spectrum fatigue lifetime prediction is very sensitive to changes in the Goodman Diagram at high R-values (approaching 1.0). The present study has added R-values between 0.5 and 1.0 to the existing Goodman Diagram developed in previous studies [2, 3], using the same material.

### **Experimental Methods**

The material used in the study is listed as DD16 in the DOE/MSU Database [15]. It is a typical structural laminate with a  $[90/0/\pm 45/0]_s$  layup, where the  $0^\circ$  and  $90^\circ$  plies are Owens Corning D155 E-glass stitched unidirectional fabric, and the  $\pm 45^\circ$  plies are DB120 stitched fabric. The resin was the ortho-polyester

CoResyn 63-AX-051, with a fiber volume fraction of 0.36. Material processing (by RTM), specimen geometry, and test protocol are described in detail in the database [15] and in References 1-3.

### **Results and Discussion**

The Goodman Diagram used in earlier studies [2, 3] is shown in Figure 13. The constant amplitude data are fit by a power law equation and do not include the static (one-cycle) strength data. The R-values used to construct this diagram were 0.5, 0.1, -1.0, 10 and 2, as well as the static ultimate tensile and compressive strengths, run at a displacement rate which was consistent with the fatigue tests.

Figure 14(a) includes constant amplitude S-N data for R-values 0.1, 0.5, 0.7, 0.8, and 0.9. The new data at higher R-values show unexpected trends, relatively flat at high stress, then steeper (similar to those for  $R=0.1$  and 0.5) at lower stresses. The trends for maximum stresses below 450 MPa have been fit to a power law relationship (Equation 2) not including the higher stress data. These data for  $R=0.7, 0.8,$  and  $0.9$  are replotted in Figure 14(b) as a function of total test time, rather than cycles; constant load data ( $R=1.0$ ) are added to this plot. The less steep, higher stress portion of the cyclic data falls in a similar range to the  $R=1.0$ , stress-rupture data.

The lower stress trend lines in Figure 14(a) are steeper than expected from interpolation on the Goodman Diagram in Figure 13. Thus, a Goodman Diagram including these new data will indicate shorter lifetimes in the low amplitude regime. Figure 15 is an expanded Goodman Diagram plot of the tensile domain for  $10^4$  and  $10^6$  cycle lifetimes. Lifetimes of between one and two decades shorter are evident for the new lines, as compared with those based only on R-values of 0.1 or 0.1 and 0.5. The changes would be similar to the  $R=0.1$  case for a Goodman Diagram based only on  $R=-1$  and UTS data, as in Reference 11. While spectrum fatigue predictions have not yet been run with the new data, improvements are anticipated in both the agreement of measured and predicted lifetime using WISPERX [2, 3] and differences between WISPER and WISPERX, where the lowest amplitude cycles were removed from WISPER to form WISPERX [11].

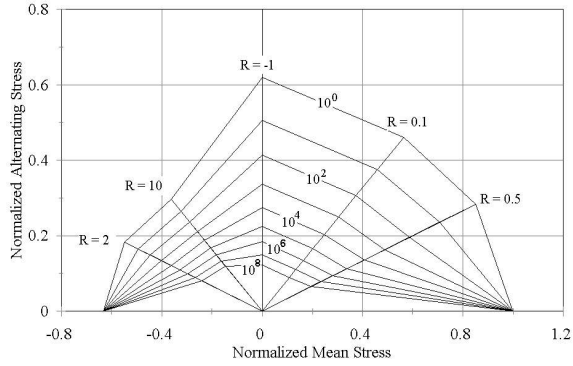


Figure 13. Goodman Diagram Based Upon Power Law Regression Analysis, Excluding Static Data [2, 3].

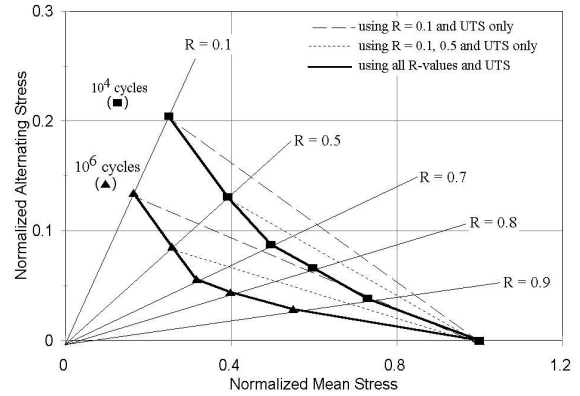


Figure 15. Tensile Regime of Goodman Diagram Showing Effects of Using Different R-Values at  $10^4$  and  $10^6$  Cycles.

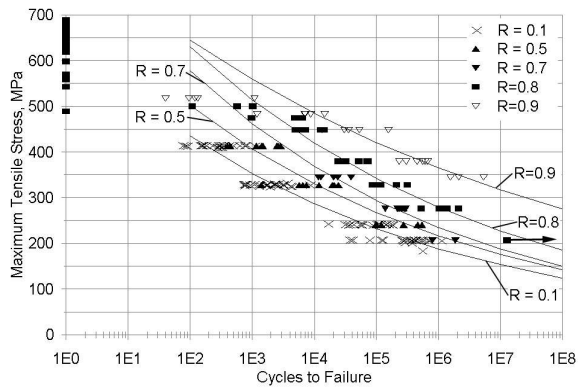


Figure 14(a). S-N Data for Tensile Fatigue at R-Values 0.1, 0.5, 0.7, 0.8 and 0.9, Database Material DD16.

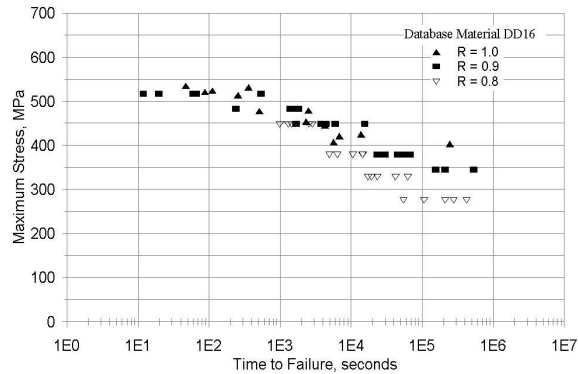


Figure 14(b). R=1.0, 0.9 and 0.8 Data for Material DD16 in Terms of Total Test Time to Failure.

## EFFECTS OF FIBER WAVINESS

### Introduction

Fiber waviness has long been recognized as a major flaw in composite materials. While severe levels of waviness, such as that associated with fiber wash in resin infusion processes, can reduce tensile strength significantly, the major impact is on compressive strength. Compressive strength is reduced due to two factors: first, the fibers are already in a buckled configuration, which is the major mode of compressive failure, and second, the fibers are misoriented, which produces the severe strength reduction associated with matrix dominated failure in off-axis materials [5]. Emerging large-tow carbon fabrics (Figure 16) appear particularly prone to developing waviness, and their compressive strength is already marginal, as discussed later.

### Waviness Inherent in Fabrics

Many stitched and woven reinforcing fabrics inherently contain fiber waviness which reduces their compressive strength; typical cases are shown in Figure 16. As indicated in Table 1, glass laminates prepared using fabrics which contain waviness have compressive strength reduced to as little as half that of D155 fabric, which has very straight fibers. This level of waviness is usually not enough to reduce the tensile strength. Carbon fabrics show similar effects, comparing the stitched and woven fabrics.

An extreme case of waviness was encountered when a single layer, unidirectional Fortafil 652 carbon fiber fabric laminate was resin transfer molded ( $V_F \sim 0.40$ ). The extreme waviness shown in Figure 17 was a

combination of inherent waviness in the fabric (Figure 16) and waviness introduced in the resin transfer process. The tensile strength of this laminate was 329 MPa. When this fabric was molded between layers of  $\pm 45$  glass fabric [ $\pm 45(G)/0_3(C)/\mp 45(G)$ ], the tensile strength increased to 764 MPa, as the off-axis layers tend to hold the  $0^\circ$  layers straighter.

### Introduced Waviness

In-plane waviness may result from fiber wash in resin-infusion or other processes. A study has been carried out to explore the effects of in-plane waviness by controllably introducing waves to an otherwise straight fiber fabric (D155)[16]. While several geometries were explored, the results here relate to laminates in the configuration  $[0/\pm 45/0]_s$ , with D1550's and DB120  $\pm 45$ 's. The waviness was introduced to all  $0^\circ$  layers at the same location (Figure 18). The primary resin was the ortho-polyester described earlier, and a toughened vinyl ester (Derakane 8084) was used for comparison.

Waves with different wave severity (as defined in Figure 19) were introduced by hand to the fabric [16]. Wave severity is the ratio of wave amplitude,  $\delta$ , to wave length,  $\lambda$ . The waves were also characterized by the degree of misorientation,  $\theta$ , also shown in Figure 19. A modified grip with lateral restraint was used to compression test the specimens, so that the gage section was of adequate length to include the wave, without elastic buckling [16].

The compressive strength as a function of wave severity is given in Figure 20 for the two resins. The waviness produces a strength loss exceeding 50 % of the baseline value for severe waviness, with only a slight improvement for the tough resin. These and other data show that compressive strength correlates with wave severity rather than wave length or amplitude separately, consistent with literature reports for carbon epoxy prepreg laminates [17]. Figure 21 shows that the data for laminates with introduced waviness have a very similar trend to that for laminates which contain only layers at  $\pm\theta$ , where  $\theta$  is the maximum angle in the wave (Figure 19). The  $\pm\theta$  data are from the DOE/MSU database [5, 15]. Figure 22 shows the failure mode for several test specimens.

The fatigue resistance was determined for a particular case of severe waviness. Figure 23 compares data for the laminates with waviness in the D155- $0^\circ$  layers with those for a woven fabric, A130, with waviness inherent in the weave. Waviness in the D155 layers reduces the static compressive strength to slightly

below the value for the A130 laminates. The fatigue trends are similar for all three cases if the stress is normalized by the static strength [16].

Tensile tests showed no measurable drop in tensile strength for mild waviness (severity = 0.107), but a drop of about 40 percent for severe waviness (severity = 0.168) [16].

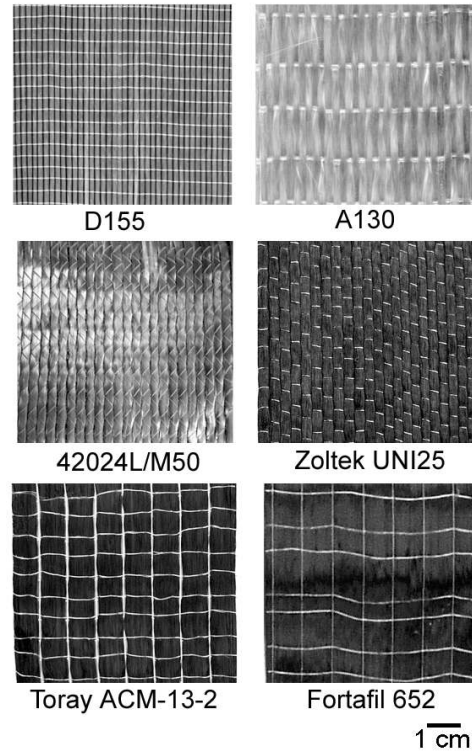


Figure 16. Dry Fabric Samples.

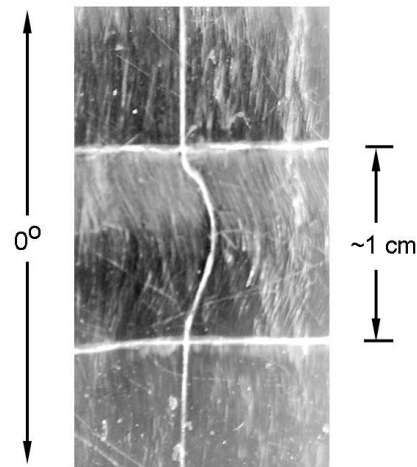


Figure 17. Fiber Waviness in a Unidirectional Carbon Ply (Fortafil 652).

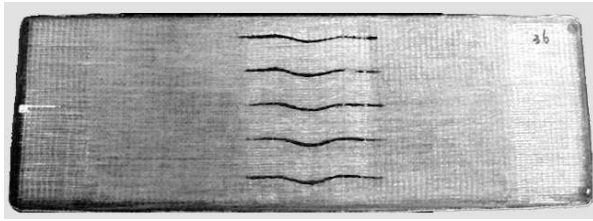


Figure 18. Laminate with Introduced Waviness.

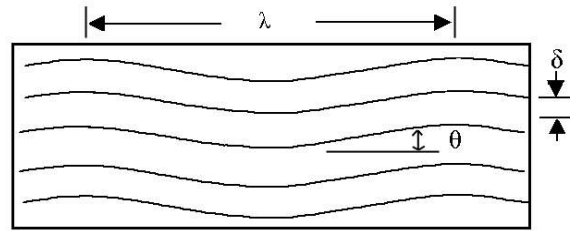


Figure 19. Waviness Characterization.

Table 1. Static Compressive Strength of Laminates Using Commercial Fabrics (Figure 16) which Containing Varying Amounts of Waviness in  $0^\circ$  layers (all non- $0^\circ$  layers are  $\pm 45^\circ$  DB 120 glass fabric).

Database Designation	$0^\circ$ Layers	% $0^\circ$	$V_{F_1}$ %	Resin	Compressive Strength, MPa	Compressive Strain to Failure, %	Remarks
DD5P	D155	72	37	Polyester	574	2.4	glass, stitched straight strands
DD8	D155	72	44		582	2.1	
DD11	A130	68	30		319	1.6	glass, woven strands
DD13	A130	68	46		314	1.1	
DD27A	Ahlstrom	76	32		381	1.9	glass, stitched to mat, wavy strands
DD27B	Ahlstrom	76	42		321	1.2	
CGD4	ACM-13-2	76	51	Vinyl ester	588	0.71	carbon, stitched fabrics, low waviness
CGD4E	ACM-13-2	76	51	Epoxy	684	0.81	
UNI25A	UNI25	100	45	Vinyl ester	535	0.61	woven large tow carbon

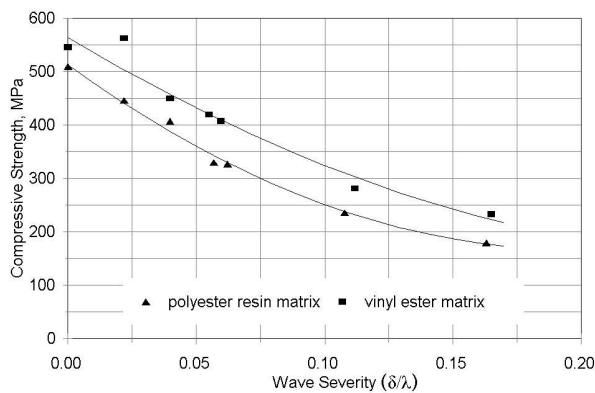


Figure 20. Effects of Resin Matrix Toughness on Compressive Strength of Laminates Containing Various Severities of Waviness.

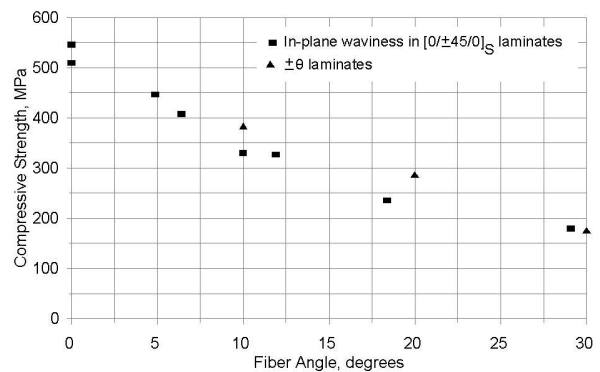


Figure 21. Compressive Strength versus Waviness Angle ( $\theta$ ) Compared with Data from  $\pm\theta$  Off-Axis Laminates.

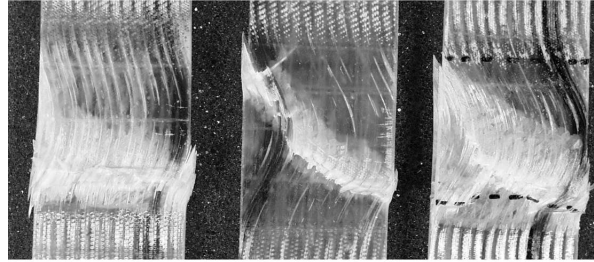


Figure 22. Static Compression Failures and Fatigue Compression Failures (left: static/ vinyl ester resin; center: static/polyester resin; right: fatigue/polyester resin)

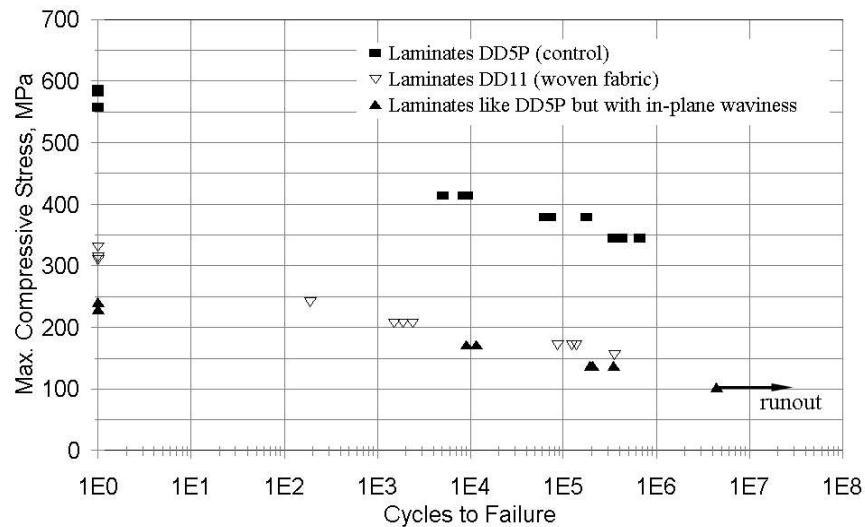


Figure 23. Compressive Fatigue Properties for Laminates with 4 mm / 35 mm ( $\delta/\lambda$ )Waviness Compared with Woven Fabric Laminate (DD11) and Control for Waviness Study (DD5P), R=10.

## FATIGUE OF LARGE TOW CARBON AND HYBRIDS

### Introduction

Carbon fibers have the potential to improve the efficiency of blade designs due to their increased modulus and strength and reduced density and tensile fatigue sensitivity relative to glass fibers. The potential of carbon fibers depends strongly on their price, which has been dropping as production shifts to larger tow (strand) sizes. Carbon fiber composites have been the subject of intense research for many years due to their attractiveness for aerospace applications, and an extensive database of static and fatigue properties is available in the open literature [17]. However, few data are available for the new, lower-cost large-tow forms of

carbon fibers, particularly in fabrics, or for matrix materials of interest in blade applications.

The advent of larger tow, lower cost carbon fiber materials in both prepreg and woven fabric (Figure 16) forms has led to the possibility of economical laminates which are all carbon or at least all carbon in the 0° plies. On-going tests are designed to investigate the potential of these materials for blade applications. This section provides results and discussion for the materials tested to date, but a full set of data is not yet available.

### Results and Discussion

Literature fatigue data [18] for small-tow carbon fiber/epoxy prepreg composites indicate much improved tensile fatigue resistance over glass fiber composites; the fatigue coefficient,  $b$ , in the exponential

relationship (Equation 1), is usually in the range of 0.04 compared with 0.10 to 0.14 for all glass fiber composites. Compression fatigue data for carbon[19] are similar to those for glass, with b-values in the 0.07 to 0.08 range. Both tensile and compressive ultimate strengths are usually higher than for glass, while corresponding strain values are lower.

Figures 24 and 25 give tensile and compressive stress and strain based fatigue data, respectively, for a large-tow carbon fiber unidirectional composite (UNI25 in Figure 16) with a vinyl ester matrix, fabricated by RTM. The tensile data are in the expected range for both static strength and ultimate strain, and fatigue coefficient, b. The compression ultimate strength and strain results are relatively low (Table 1), apparently due to the fabric weave (as noted earlier, woven glass fiber composites have lower compressive properties than do straight-fiber stitched fabrics or preregs). The compressive ultimate strain is in the range of 0.6 percent, and fatigue strains at  $10^6$  cycles are in the 0.4 percent range. A similar fabric, UNI21, produced somewhat lower results, but the loose weave resulted in significant fiber wash during processing. Table 2 gives unidirectional elastic and strength properties for a large tow carbon fiber system compared with common glass fiber materials.

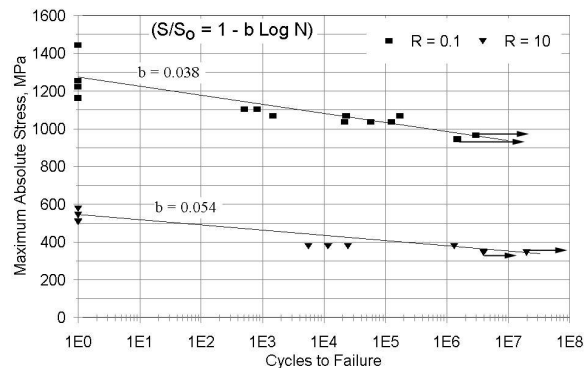


Figure 24. S-N Diagram for Large Tow Unidirectional 0° Carbon Fiber/Vinyl Ester Composites (UNI25 and UNI25A in the Database), R = 0.1 and 10.

Large tow carbon/epoxy prepreg data given by material suppliers show compression ultimate strain values above 1.0 percent [20]. It is expected that stitched fabric performance, possibly with an epoxy resin, might also reach the 1.0 percent range if waviness and fiber misalignment are minimized. Whether large blades can be manufactured without significant fiber waviness remains to be seen; experience with carbon

fabrics in the RTM process at MSU has been that it is difficult to obtain good quality laminates without some fiber waviness.

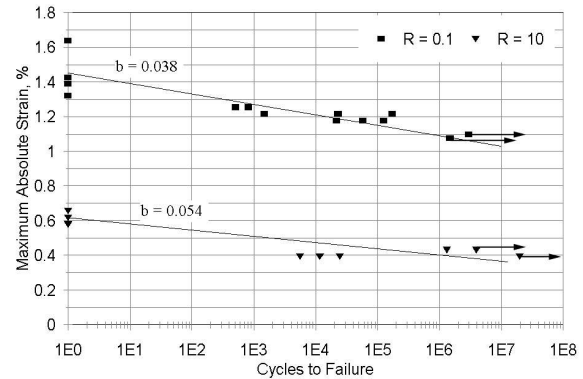


Figure 25. Fatigue Strain Diagram for Large Tow Unidirectional 0° Carbon Fiber/Vinyl Ester Composites (UNI25 and UNI25A in the Database), R = 0.1 and 10,  $V_F=0.40$ .

The likely scenario for hybrid carbon/glass composites is to use all carbon in the 0° layers, with glass in the less critical  $\pm 45^\circ$  layers. This should reduce the cost relative to all carbon composites, while providing nearly the same tensile and compressive strength, stiffness, and fatigue resistance as an all carbon laminate. The shear stiffness and buckling resistance would be reduced by use of the glass off-axis materials. Figure 26 provides data for strain versus cycles to failure in compression fatigue for composites in the configuration  $(\pm 45_G/0_{3C}/\mp 45_G)$ , with glass  $\pm 45^\circ$  plies and Toray large tow stitched carbon fabric ACM-13-2 0° plies (Figure 16). The figure shows that the epoxy matrix provides somewhat improved compressive strength and fatigue resistance relative to vinyl ester. The results with the vinyl ester matrix show moderate improvement over the woven large tow carbon data in Figure 25, with further improvement using the epoxy matrix. The Toray fabric (Figure 16) still contains some fiber misalignment and waviness relative to smaller tow carbon.

## Conclusions

Small strand tensile fatigue data have been generated out to  $10^{10}$  cycles with a speaker cone apparatus. The results show much higher static strength and fatigue resistance than for conventional coupons (in the moderate cycle range). The fatigue data support the use of a power law representation. Only small improvements are found at high cycles with a

toughened resin.

Additions to the Goodman Diagram show shorter than expected lifetimes at low amplitudes. These data may reduce predicted spectrum fatigue lifetimes, bringing them into closer agreement with experiments.

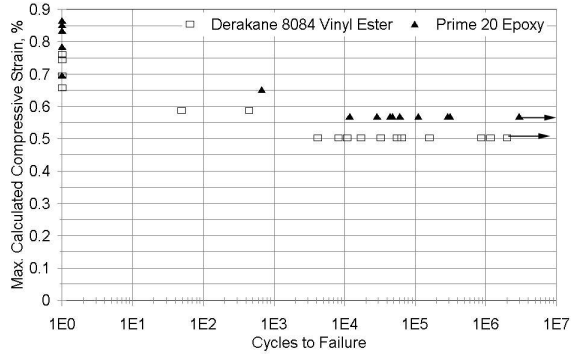


Figure 26. Compression Fatigue Data for Hybrid Laminates with Vinyl Ester and Epoxy Matrices, Material CGD4 with a Ply Configuration ( $\pm 45_G/0_{3C}/\mp 45_G$ ),  $0^\circ$  Fabric is Toray ACM-13-2 Carbon and  $\pm 45^\circ$  Fabric is DB120 Glass, 76 Percent  $0^\circ$  Material by Volume,  $V_F=0.50$ ,  $R=10$ .

Fiber waviness can be a major flaw in composite structures, particularly with large tow carbon fibers using infusion methods. Data show a systematic reduction in compressive strength as wave severity increases. Tensile strength is affected only by severe waviness.

Early data for large tow, low cost carbon fiber composites show good tensile fatigue performance, but marginal compression fatigue performance. The compression static and fatigue data are lowest for the woven fabrics, and improve for stitched fabrics. Prepreg composites with large tows and epoxy resins provided improved performance. The compression results indicate that caution should be exercised in using these fabrics for blade applications; further testing and full consideration of statistics and knockdown factors are needed to gain confidence with the large tow carbon fiber materials. In infusion processes, the possible introduction of severe waviness requires careful monitoring.

Table 2. Elastic Constants for Glass and Large Tow Carbon Unidirectional Fabrics ( See Reference 15 for testing details and Symbol Definitions).

			Longitudinal Direction								Transverse Direction				
			Elastic Constants				Tension		Compression		Shear	Tension		Compression	
Fabric	lay-up	$V_F$ %	$E_L$ GPa	$E_T$ GPa	$\nu_{LT}$	$G_{LT}$ GPa	$UTS_L$ MPa	$\epsilon_U$ %	$UCS_L$ MPa	$\epsilon_U$ %	$\tau_{TU}$ MPa	$UTS_T$ MPa	$\epsilon_U$ %	$UCS_T$ MPa	$\epsilon_U$ %
A130 Glass	$[0]_8$	45	36.3	8.76	0.32	3.48	858	2.53	-334	-0.92	85.3	33.8	0.39	-93.3	-1.05
D155 Glass	$[0]_6$	45	35.0	8.99	0.31	4.10	987	2.83	-746	-2.02	97.7	27.2	0.32	-123	-1.67
UNI25 Carbon	$[0]$	45	89.7	6.80	0.27	2.36	1213	1.35	-535	-0.60	30.0	20.5	0.31	-100	-1.47

**REFERENCES**

1. Wahl, N, Samborsky, D.D., Mandell, J.F., and Cairns, D.S., Proceedings of the 2001 ASME Wind Energy Symposium, ASME/AIAA, New York, pp. 49-59. (2001)
2. Wahl, N.K, Mandell, J.F., Samborsky, D.D., "Spectrum Fatigue Lifetime and Residual Strength for Fiberglass Laminates," Contractor Report SAND2002-0546, Sandia National Laboratories, Albuquerque, NM, 2002.
3. Wahl, N, Samborsky, D.D., Mandell, J.F., and Cairns, D.S., Proceedings of the 2002 ASME Wind Energy Symposium, ASME/AIAA, New York, pp.19-26. (2002)
4. Mandell, J. F., Samborsky, D. D., and Cairns, D. S, "Fatigue of Composite Materials and Substructures for Wind Turbine Blade," Contractor Report SAND2002-077, Sandia National Laboratories, Albuquerque, NM, 2002.
5. Mandell, J.F. and Samborsky, "DOE/MSU

- Composite Material Fatigue Database: Test Methods, Materials, and Analysis," Contractor Report SAND97-3002, Sandia National Laboratories, Albuquerque, NM (1997).
6. Mandell, J.F., McGarry, F.J., Hsieh, A.J.-Y and LI, C.G., Reinforced Plastics Composites Institute, Society of the Plastics Industry, Paper 7-G, 1985.
  7. Mandell, J.F., Huang, D.D., McGarry, F.J., Composites Technology Review, Vol. 3, No. 3, 1981, pp. 96-102.
  8. Samborsky, Daniel, D. "Fatigue of E-glass Fiber Reinforced Composite Materials and Substructures," M.S. Thesis, Department of Civil Engineering, Montana State University, 1999.
  9. Samborsky, D.D. and Mandell, J.F., "Very High Cycle Tension Fatigue of Impregnated E-glass Strands" (to be published)
  10. Mandell, J.F., Samborsky, D.D., Li, M., Orozco, R., and Cairns, D.S., Proceedings of the 2000 ASME Wind Energy Symposium, ASME/AIAA, New York, pp. 354-366. (2000)
  11. van Delft, D. R. V., de Winkel, G. D., and Joossee, P. A., in Proc. 1997 ASME Wind Energy Symposium, ASME, AIAA, New York, pp. 180-189 (1997).
  12. Echtermeyer, A. T., Kensch, C., Bach, P., Poppen, M., Lilholt, H., Andersen, S. I., and Brøndsted, P., Proceedings of 1996 European Union Wind Energy Conference, 1996.
  13. Nijssen, R.P.L., van Delft, D.R.V., van Wingerde, A.M., in Proceedings 2002 ASME Wind Energy Symposium, ASME/AIAA, New York, pp.10-18 (2002).
  14. Solin, J., "Methods for Comparing Fatigue Lives for Spectrum Loading," International Journal of Fatigue, Vol. 12, No. 1, 1990.
  15. Mandell, J.F. and Samborsky, D.D., "MSU/DOE Wind Turbine Blade Composite Material Fatigue Database," February 2002, Sandia National Laboratories, Albuquerque, NM, 87185. Updates available at [www.sandia.gov/Renewable\\_Energy/wind\\_energy/other/973002upd0202.pdf](http://www.sandia.gov/Renewable_Energy/wind_energy/other/973002upd0202.pdf).
  16. Wang, Lei, "Effects of In-plane Fiber Waviness on the Properties of Composite Materials," M.S. Thesis, Department of Chemical Engineering, Montana State University, 2001
  17. U. S. Department of Defense, "The Composite Materials Handbook," MIL-17 Mil-HDBK-17-1F, January, 1997. ([www.mil17.org](http://www.mil17.org))
  18. Mandell, J.F., "Fatigue Behavior of Short Fiber Composite Materials (Ch. 7)," The Fatigue Behavior of Composite Materials, K.L. Reifsnider, Ed., Elsevier (1990).
  19. Grimes, G.C., "Test Methods and Design Allowables for Fibrous Composites," ASTM 734, C.C. Chamis, ed., ASTM, Phil., 1981, pp.281-337.
  20. Personal Communication, R. Yamamoto, Toray Industries, Inc.